Electro-Hydrodynamic (EHD) Thrust Analysis in Wire-Cylinder Electrode Arrangement

Konstantinos N. KIOUSIS[1], Antonios X. MORONIS[2], Wolf G. FRUH[1]

[1]Heriot-Watt University, Edinburgh EH14 4AS, UK
[2]Technological Educational Institute (TEI) of Athens, Aegaleo 12210, Greece

Abstract The thrust generation by electro-hydrodynamic (EHD) effect has been studied for a wire-cylinder arrangement under high DC voltage. Series of measurements have been conducted in order to determine the relationship between generated thrust and corona discharge current, as well as its dependence on geometrical characteristics of the electrodes, e.g. electrode gap, wire and cylinder radii. The experimental investigation has shown a linear relationship between the generated thrust and the discharge current, while parametric analysis showed that increased electrode gap and emitter radius reduces the thrust. On the other hand, large gaps favor the thrust per unit power ratio.

Keywords: electro-hydrodynamic (EHD) effect, thrust, wire-cylinder electrodes

PACS: *47.65.−d, 52.80.−s, 52.30.−q*

DOI: 10.1088/1009-0630/16/4/11

(Some figures may appear in colour only in the online journal)

1 Introduction

It is widely accepted in literature that an electro-hydrodynamic (EHD) effect appears when high voltage is applied across a pair of electrodes having substantially different radii of curvature e.g. a sharply pointed electrode (emitter) and a larger radius electrode (collector) [1,2]. The high intensity of the electric field in the vicinity of the electrode with the smaller radius causes gaseous ionization in the surrounding air. The onset of corona discharges results in space charge accumulation, which, in turn, produces current flow (corona discharge current) as the molecules of ionized air drift towards the collector. During their motion, charged ions collide with neutral air molecules and atoms which lie along their path, thus transferring their momentum and generating a flow towards the collector, known as "ionic" or "electric" wind [3]. At the same time a unidirectional thrust appears in the direction towards the emitter, regardless of the electrode polarity. The resulting force seems to be proportional to the amount of energy stored in the electric field in the area between the two electrodes [4]. The EHD effect has many industrial and research applications [5−10]. Other potential applications may include flow control [11], drag reduction [12] and turbulence transition delay [13], as well as dielectric pumping [14] and enhancement of heat transfer in cooling [15,16]. Recently, significant research has been conducted for propulsion applications [17−23] or for the optimization of the EHD flow characteristics [24,25] within the narrow range between the corona inception voltage and the breakdown voltage of the gap between the electrodes [26]. According to the bibliography [11,23−25,27] positive coronas have been proved to be more efficient than negative ones.

In this work, the generated EHD flow has been studied for the arrangement of a thin wire parallel to a conducting cylinder of significantly larger diameter. This electrode setup has been selected because of the strongly inhomogeneous field that can be produced during high-voltage application, which, in turn, is capable of generating significant EHD flow.

2 Experimental setup

In order to study the wire-cylinder arrangement, experimental modules were carefully prepared. Each module consisted of a thin polished copper wire with radius r (emitter) and an aluminum cylinder (collector) with radius R, while both electrodes were 300 mm long. Fixed on a polyethylene frame, the two electrodes were placed parallel to each other at a distance of d in atmospheric air.

As shown in Fig. 1, the whole construction hung freely by a thin cotton thread, which was available at the bottom of a precision balance. The balance stand, containing the electrode setup, was isolated from outside air disturbances by the use of detachable Plexiglas covers, which formed in this way a closed box. This arrangement ensured undisturbed EHD flow between the electrodes.

An adjustable 40 kV high voltage source (Matsusada

Precision W Series) supplied the emitter with positive DC voltage, while the collector was connected to the electrical ground. The positive corona discharge current was measured by a Metra Hit 28S precision multimeter connected in series between the collector and the ground, while the thrust generated by the EHD effects was detected and measured as a reduction in weight of the electrode system with a Kern 572-32 precision electronic balance with 1 mg resolution.

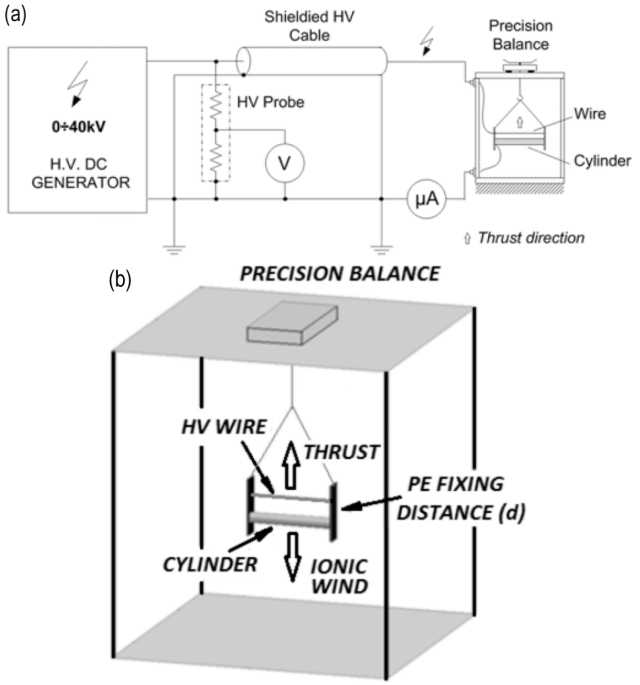

Fig.1 (a) Schematic of the experimental setup and (b) perspective view of the electrode setup with supporting construction

3 EHD thrust model

According to the bibliography, EHD flow is directly related to the onset of corona discharges, above a critical value of the electric field strength. On the other hand, high field homogeneity is required to confine these discharges locally in the vicinity of the sharper electrode, thus avoiding undesirable breakdowns [28−30]. In our case, the corona current, flowing from the wire towards the grounded cylinder, generates an air flow (ion wind) in the same direction, as moving positive ions collide with neutral air molecules, exchanging their momentum and, finally, accelerating them.

The generated thrust is in fact a reaction force against the field force, so it can be approximated by the sum of all electric field forces acting on moving ions as follows [30]:

$$F = n_{\mathrm{i}} \cdot A \cdot d \cdot e \cdot E, \tag{1}$$

where n_{i} is the ion density, A [m^2] is the discharge cross section, d is the gap length [m], e is the unit charge (charge of an electron) and E [V/m] is the average electric field .

The total charge Q can then be expressed as:

$$Q = N \cdot e, \tag{2}$$

and the discharge current expressed as :

$$I = \frac{\mathrm{d}Q}{\mathrm{d}t} = \frac{\mathrm{d}}{\mathrm{d}t}(n_{\mathrm{i}} \cdot A \cdot d \cdot e) = \frac{\mathrm{d}}{\mathrm{d}t}(n_{\mathrm{i}} \cdot A \cdot u \cdot \mathrm{d}t \cdot e)$$
$$= n_{\mathrm{i}} \cdot A \cdot u \cdot e = n_{\mathrm{i}} \cdot A \cdot \mu \cdot E \cdot e. \tag{3}$$

From Eqs. (1), (3) we finally obtain the following expression [30]:

$$F = \frac{d}{\mu} \cdot I, \tag{4}$$

where F [N] is the generated thrust, I [A] is the corona discharge current, d [m] is the electrode gap and μ is the ion mobility (1.8-2.2×10^{-4} m^2/V·s in air) [31,32].

Eq. (4) represents the relation between the generated thrust and the corona discharge current in a uniform electric field with a constant discharge cross section A. In the case of a wire-cylinder arrangement, the electric field is not uniform along the axis of the gap, so the discharge cross section is a function of the distance between the wire and the cylinder. Thus the thrust could be expressed as:

$$F_{\mathrm{w-c}} = n_{\mathrm{i}} \cdot A(d) \cdot d \cdot e \cdot E_{\mathrm{av}} = n_{\mathrm{i}} \cdot V_{\mathrm{w-c}} \cdot e \cdot E_{\mathrm{av}}, \tag{5}$$

where $V_{\mathrm{w-c}}$ [m^3] represents an 'equivalent' ionic flow volume (see Fig. 2) and E_{av} [V/m] is the average electric field intensity within this volume.

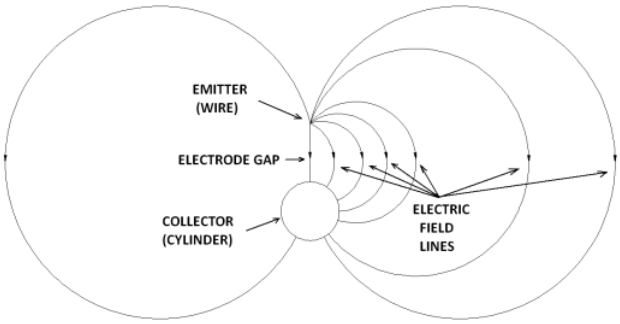

Fig.2 Graphical representation (on plane) of the moving ions trajectories along the field lines, which define the boundaries of the ionic flow volume

Combining Eqs. (4) and (5), we have:

$$F_{\mathrm{w-c}} = f \cdot \frac{d}{\mu} \cdot I. \tag{6}$$

In the above equation f is introduced as a 'field coefficient' for the wire-cylinder arrangement, defined as:

$$f = \frac{V_{\mathrm{w-c}}}{V_{\mathrm{hom}}} \cdot \frac{E_{\mathrm{av}}}{E_{\mathrm{hom}}}. \tag{7}$$

Here V_{hom} [m^3] is the ionic flow volume that should be considered for a homogeneous electric field (e.g. between parallel plates) across the same gap d and voltage V, where the average field strength E_{hom} would be equal to the ratio V/d. It should be noted that f could be considered as a measure of the electric field inhomogeneity and equals 1 for a totally homogeneous electric field.

4 Corona current distribution

The corona current distribution in space is controlled by the applied electric field flow lines (see Fig. 2). These flow lines define ion trajectories starting from the wire and terminating at the cylinder's surface, with incidence angle θ.

Assuming single carrier conduction in air, the distribution of saturated current density $j(\theta)$ over the cylinder's surface can be approximated by the following formula [27]:

$$j(\theta) = \mu \cdot \varepsilon_0 \cdot \frac{V^2}{L(\theta)^3}, \tag{8}$$

where $j(\theta)$ is the saturated current density over the cylinder's surface [A/m^2], as a function of the incidence angle θ (see Fig. 4), ε_0 is the dielectric permittivity of air (8.85×10^{-12} F/m) and $L(\theta)$ [m] is the total drift distance of the ions along every single trajectory.

The corona current distribution on the cylinder versus angle θ can be estimated by integrating Eq. (8) as follows:

$$I(\theta) = 2 \cdot \int_0^{\theta} \mu \cdot \varepsilon_0 \cdot \frac{V^2}{L(\theta)^3} \cdot R\mathrm{d}\theta. \tag{9}$$

The total current per unit electrode length can be estimated for $\theta = \pi$.

Dedicated multiphysics modeling software has been implemented to determine $L(\theta)$ in each case and then $I(\theta)$ according to Eq. (9). Fig. 3 shows the results of the normalized current density distribution over the cylinder's surface, which follows the well-known Warburg law [33], as well as the normalized current versus the angular displacement.

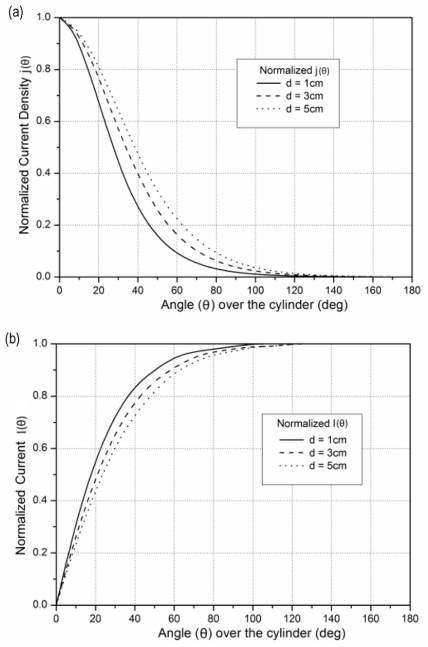

Fig.3 (a) Normalized current density distribution $j(\theta)$, over the cylinder with angular displacement and (b) normalized current $I(\theta)$ with angular displacement (d= 1 cm, 3 cm and 5 cm, r = 50 μm and R=15 mm). Similar results can be obtained for other r and R values

It can be seen that the contribution of the current density for incidence angles over 80° is minimal. So, the trajectories with incidence angle equal to 80° could be considered as the boundaries of the 'active' flow region (see Fig. 4). In this way, the 'active' flow volume can be estimated by finite element analysis considering the volume surrounded by these trajectories.

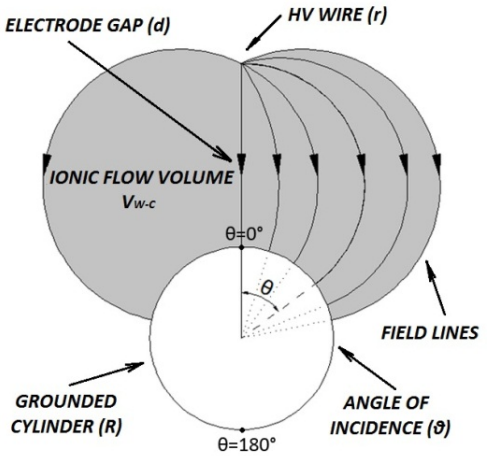

Fig.4 Representation of the field lines, which define the boundaries of the 'active' flow volume $V_{\mathrm{w-c}}$ (Grey part)

5 Experimental results and discussion

Series of measurements were carried out to determine the relation between generated thrust and discharge current, as well as the dependence of the thrust and field coefficient f on electrode gap d and emitter and collector radii r and R, respectively, while the electrode length was kept unchanged at 300 mm in all cases.

The experimental investigation was conducted in a controlled lab environment with temperature and relative humidity almost constant at 25 °C and 45%, respectively, while the measurements of the generated thrust were performed by applying high DC voltage to the emitter electrode at 1 kV increments, above the corona inception threshold.

5.1 Influence of the electrode gap d

Investigation of the generated thrust was carried out on three modules with electrode gap d_1=20 mm, d_2=30 mm and d_3=40 mm, while the emitter and collector radii were 50 μm and 15 mm, respectively. Plots of the generated thrust per unit electrode length are presented versus the applied voltage and the corona discharge current in Fig. 5(a) and (b) respectively.

Field coefficient f was derived from the experimental results (Fig. 5(b)), by applying a least square fit to Eq. (6). The average electric field intensity E_{av} and the 'active' ionic flow volume $V_{\mathrm{w-c}}$ were determined by finite element analysis, considering the volume surrounded by the electric field lines with incidence angles

up to $\theta_{\max}$=80° (see Fig. 4). The equivalent homogeneous ionic flow volume was derived in each case according to Eq. (7). All the above results are summarized in Table 1.

Table 1. Field coefficient f and ionic flow volumes $V_{\mathrm{w-c}}$ and V_{hom} versus electrode gap d for r=50 μm and R=15 mm

Electrode gap d (mm)	Field coefficient f	$V_{\mathrm{w-c}}$ (cm^3)	V_{hom} (cm^3)
$d_1 = 20$	0.541	484	868
$d_2 = 30$	0.600	656	1050
$d_3 = 40$	0.674	1065	1406

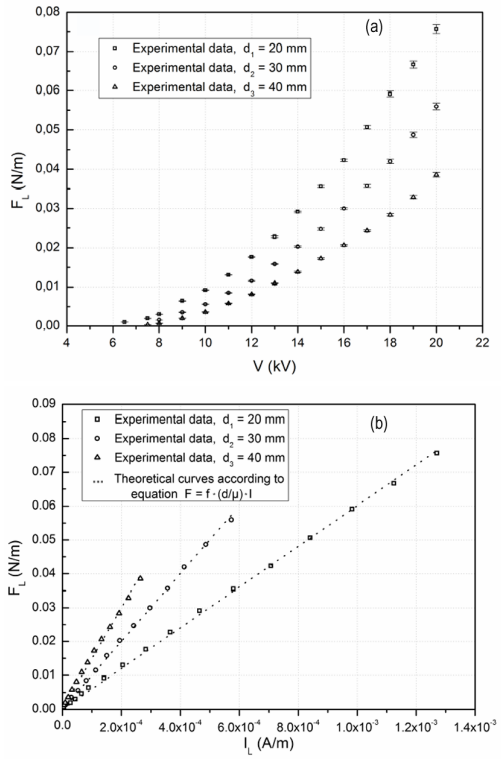

Fig.5 Generated thrust per unit length [N/m] versus (a) applied voltage and (b) discharge current [A/m] (d_1=20 mm, d_2=30 mm and d_3=40 mm, r=50 μm and R=15 mm)

As shown in Fig. 5, the generated thrust reduces with gap distance d, but on the other hand, the field coefficient f increases with d. This is reasonable, since larger gaps produce more homogeneous electric fields ($f \to 1$).

5.2 Influence of the emitter radius r

The dependence of the generated thrust on the emitter electrode radius r was also investigated, with measurements of the thrust on three modules with r_1=50 μm, r_2=100 μm and r_3=250 μm, while the electrode gap d and the collector electrode radius R were kept unchanged at 30 mm and 15 mm, respectively. In this case also, fitting curves were drawn according to Eq. (6). The average electric field intensity E_{av}, the ionic flow volume $V_{\mathrm{w-c}}$, as well as the equivalent homogeneous ionic flow volume V_{hom}, were also determined as in the previous section. The results are given in Fig. 6 and Table 2, respectively.

As shown in Table 2, field coefficient f differs slightly as far as the emitter radius is concerned. This is in agreement with the small changes in the ionic flow volume, due to the fact that the emitter radius is very small in comparison with d or R, thus having a small effect on the distribution of the electric field lines in space.

Table 2. Field coefficient f and ionic flow volumes $V_{\mathrm{w-c}}$ and V_{hom} versus emitter radius r for d=30 mm and R=15 mm

Emitter radius r (μm)	Field coefficient f	$V_{\mathrm{w-c}}$ (cm^3)	V_{hom} (cm^3)
$r_1 = 50$	0.600	656	1050
$r_2 = 100$	0.597	662	997
$r_3 = 250$	0.594	689	985

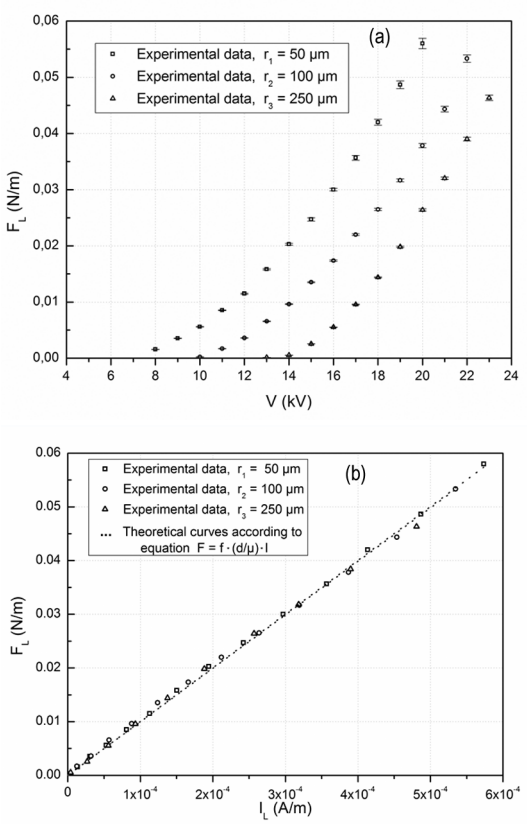

Fig.6 Generated thrust per unit length [N/m] versus (a) applied voltage and (b) discharge current [A/m] (r_1=50 μm, r_2=100 μm and r_3=250 μm, d=30 mm and R=15 mm)

5.3 Influence of the collector radius R

Measurements of the generated thrust were performed on three modules with R_1=5 mm, R_2=10 mm and R_3=15 mm, for the purpose of defining the dependence of the thrust on the collector electrode radius, while the electrode gap d and the emitter electrode radius r were kept unchanged at 30 mm and 50 μm, respectively (see Fig. 7).

Fitting curves were drawn to determine the field coefficient f for different cylinder radii. The average electric

field intensity E_{av}, the ionic flow volume $V_{\mathrm{w-c}}$, as well as the equivalent homogeneous ionic flow volume V_{hom}, were determined accordingly, as shown in Table 3.

It becomes clear that the collector radius R has a very small effect on the field coefficient f, but on the other hand, $V_{\mathrm{w-c}}$ and V_{hom}, increase abruptly with R, mainly because of the electric field line spread-out as R increases.

Table 3. Field coefficient f and ionic flow volumes $V_{\mathrm{w-c}}$ and V_{hom} versus collector radius R for d=30 mm and r=50 μm

Collector radius R (μm)	Field coefficient f	$V_{\mathrm{w-c}}$ (cm^3)	V_{hom} (cm^3)
R_1= 5 mm	0.583	279	436
R_2= 10 mm	0.592	528	839
R_3= 15 mm	0.600	656	1050

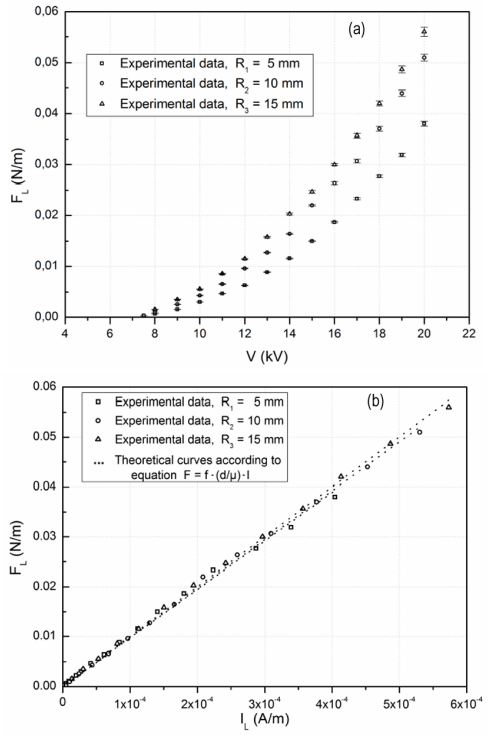

Fig.7 Generated thrust per unit length [N/m] versus (a) applied voltage and (b) discharge current [A/m] (R_1=5 mm, R_2=10 mm and R_3=15 mm, d=30 mm and r=50 μm)

5.4 Thrust per unit power, thrust efficiency and flow efficiency

Based on the above results, the generated thrust [N/m] was plotted against consumed power per unit electrode length [W/m] for various geometrical characteristics of the wire-cylinder electrode assembly (see Fig. 8).

Moreover, plots of thrust efficiency φ [N/kW] against the thrust per unit length of the electrodes [N/m] were also made for various gaps and emitter and collector radii (see Fig. 9).

It becomes clear from Figs. 8 and 9 that in terms of thrust efficiency, which is frequently used in literature as an overall performance evaluation factor [20−24,30], the electrode gap d, primarily, and the wire radius, secondarily, play the most important role in the variation of thrust per unit power ratio. The cylinder radius seems to have limited effect. The maximum value of the generated thrust (F=0.076 N/m at 20 kV) was measured for the shortest gap (d_1=20 mm), as shown in Fig. 8(a), but on the other hand, the corresponding efficiency was very low (≈3 N/kW). Although the generated thrust reduces with d, large gaps favor the thrust per unit power ratio. The maximum values of the efficiency were recorded for the larger gap d_3=40 mm (φ=23.3 N/kW), as shown in Fig. 9(a), but with very low generated thrust (≈0.002 N/m).

Small emitter radii produce higher thrust, with higher efficiency (see Fig. 8(b) and 9(b)). On the other hand, as far as the collector electrode radius is concerned, increased R resulted in increased generated thrust and thrust per unit power ratio (see Fig. 8(c) and 9(c)).

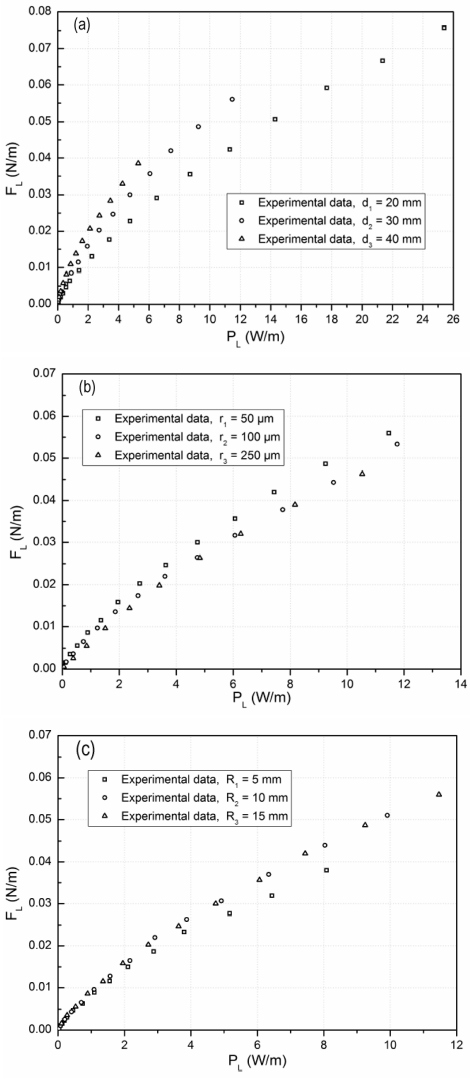

Fig.8 Generated thrust [N/m] versus power [W/m] for various geometrical characteristics: (a) variable electrode gap d, (b) variable emitter radius r and (c) variable collector radius R

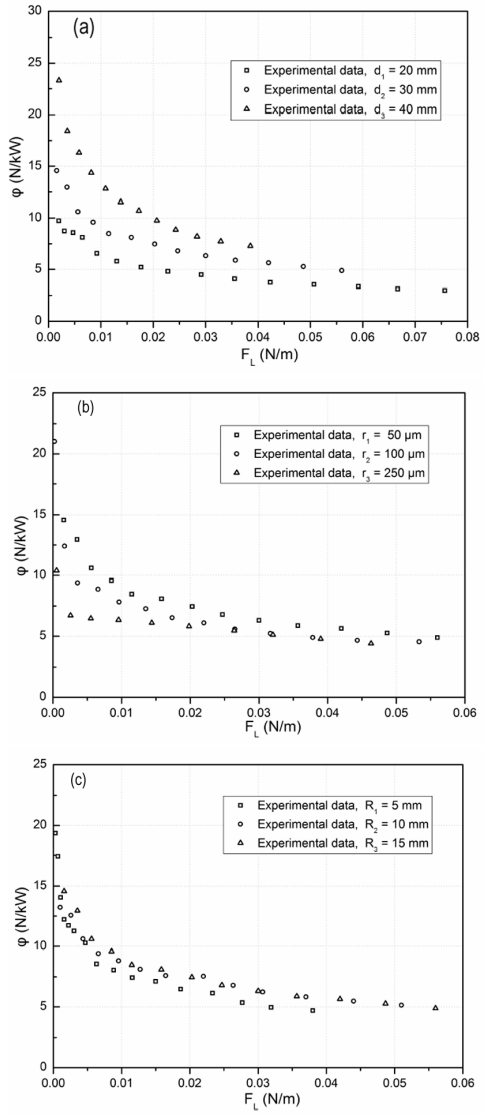

Fig.9 Thrust efficiency φ [N/kW] versus generated thrust [N/m] for various geometrical characteristics: (a) variable electrode gap d, (b) variable emitter radius r and (c) variable collector radius R

As far as the flow efficiency is concerned, it can be estimated by the following expression:

$$n = P_{\text{mech}}/V \cdot I, \tag{10}$$

where $P_{\text{mech}} = F \cdot u_{\text{EHD}}$ is the mechanical power output, F is the generated thrust [N], u_{EHD} is the ionic wind velocity [m/s], V is the applied voltage [V] and I is the corona discharge current [A].

Measurements of the ionic wind velocity in the wire-cylinder arrangement have shown that velocities up to 2.88 m/s may be reached within the range of the geometry adopted in this study [34]. In this case, the maximum electromechanical efficiency is relatively low (n=1.12%), which is however in agreement with other results found in literature for different electrode geometries [24]. Even though the wire-cylinder arrangement doesn't seem completely efficient, the thrust per unit power ratio that has been achieved was high enough compared with similar studies [20,23,30].

6 Conclusions

Theoretical and experimental investigation of the generated EHD thrust has been conducted for a wire-cylinder electrode arrangement in atmospheric air under high dc voltage. A theoretical model has been proposed based on the momentum exchanges, through collisions, between the field force-accelerated ions and the electrically neutral air molecules. A field coefficient f has been introduced to determine the generated thrust as a function of the corona current intensity. Experimental results have shown a linear relationship between the generated thrust and the corona discharge current, while parametric analysis showed that smaller electrode gaps and emitter radii result in increased thrust. On the other hand, large gaps and collector radii favor the thrust per unit power ratio. The experimental findings are in good agreement with the theoretical expectation inferred from the proposed model. The wire-cylinder setup used here seems to be quite efficient in terms of thrust per unit power ratio.

References

1 Townsend J S. 1915, Electricity in gases. Oxford University Press, New York
2 Loeb L B. 1965, Electrical coronas. University of California Press, London
3 Robinson M. 1962, A History of the Electric Wind. American Journal of Physics, 30: 366
4 Buehler D R. 2004, Journal of Space Mixing, 2: 1
5 Yamamoto T, Velkoff H R. 1981, Journal of Fluid Mechanics, 108: 1
6 Nikas K S P, Varonos A A, Bergeles G C. 2005, Journal of Electrostatics, 63: 423
7 Cloupeau M, Prunet-Foch B. 1990, Journal of Electrostatics, 25: 165
8 Jaworek A, Sobczyk A T. 2008, Journal of Electrostatics, 66: 197
9 Goldman M. 1981, IEE Proceedings A, 128: 298
10 Goldman M, Goldman A, Sigfmond R S. 1985, Pure Appl. Chem., 57: 1353
11 Moreau E. 2007, Journal of Physics D: Applied Physics, 40: 605
12 Benard N, Jolibois J, Moreau E. 2009, Journal of Electrostatics, 67: 133
13 Grundmann S, Tropea C. 2007, Journal of Experiments in Fluids, 42: 653
14 Seyed-Yagoobi J. 2005, Journal of Electrostatics, 63: 861
15 Owsenek B L, Seyed-Yaghoobi J. 1997, Journal of Heat Transfer, 119: 604
16 Huang R T, Sheu W J, Wang C C. 2009, Journal of Energy Conversion and Management, 50: 1789
17 Velasquez-Garcia L F, Akinwande A I, Martinez-Sanchez M. 2006, Journal of Microelectromechanical Systems, 15: 1260
18 Velasquez-Garcia L F, Akinwande A I, Martinez-Sanchez M. 2006, Journal of Microelectromechanical Systems, 15: 1272

19 Kirtley D, Fife J M. 2002, Modeling, simulation, and design of an electrostatic colloid thruster. The 29th IEEE International Conference on Plasma Science (ICOPS), Canada

20 Pekker L, Young M. 2011, Journal of Propulsion and Power, 27: 786, doi: 10.2514/1.B34097

21 Lin Z, Teck-Meng L. 2011, Thrust origin in EHD lifters. IEEE Industry Applications Society Annual Meeting (IAS), Orlando

22 Young M, Keith S, Pancotti A. 2009, An Overview of Advanced Concepts for Near-Space Systems. Air Force Research Laboratory, 10. E. Saturn Blvd. Edwards AFB, CA 93524, United States

23 Wilson J, Perkins H, Thompson W. 2009, An Investigation of Ionic Wind Propulsion. National Aeronautics and Space Administration (NASA) Glenn Research Center Cleveland, Ohio 44135, United States

24 Moreau E, Touchard G. 2008, Journal of Electrostatics, 66: 39

25 Matéo-Vélez J-C, Degond P, Rogier F, et al. 2008, Journal of Phys. D: Appl. Phys., 41: 1

26 Buchet B, Goldman M, Goldman A. 1966, Journal of Les Comptes Rendus de l'Académie des sciences, 263: 356

27 Robinson M. 1961, Movement of Air in the Electric Wind of the Corona Discharge. Transactions of the American Institute of Electrical Engineers, Part I: Communication and Electronics, (Volume:80 , Issue:2)

28 Stuetzer O M. 1959, Journal of Applied Physics, 30: 984

29 Robinson M. 1962, American Journal of Physics, 30: 366

30 Christenson E A, Moller P S. 1967, AIAA Journal, 5: 1768

31 Waters R T, Stark W B. 1975, Journal of Phys. D: Appl. Phys., 8: 416

32 Cooperman P. 1960, A theory for space-charge-limited currents with application to electrical precipitation. Transactions of the American Institute of Electrical Engineers, Part I: Communication and Electronics, (Volume:79 , Issue:1)

33 Warburg E. 1899, Handbuch der Physik. Springer, Berlin

34 Kiousis K N, Moronis A X. 2011, Experimental Investigation of EHD Flow in Wire to Cylinder Electrode Configuration. Proc. of 10th IASTED European Conf. (EUROPES '11), Crete, 21-26

(Manuscript received 3 December 2012)
(Manuscript accepted 14 May 2013)
E-mail address of Konstantinos N. KIOUSIS:
konstantinosq@gmail.com